Nat. Volatiles & Essent. Oils, 2021; 8(5): 4840 – 4853

Zno-Tio$_2$ Nanocomposites Synthesized By Sol-Gel Route: Study Of Their Structural And Optical Properties

[1]Sridevi K P, [2]Sivakumar S, [3] Sangeetha B, [4]Saravanan K, [5]Praveen H

[1]Department of Physics, Sri Kailash Women's College, Thalaivasal, Salem, Tamil Nadu, INDIA
[2]Department of Physics, Government Arts College (Autonomous), Salem, Tamil Nadu, INDIA.
[3]Department of EEE, AVS Engineering College, Salem, Tamil Nadu, INDIA,
[4]Department of Physics, AVS Engineering College, Salem, Tamil Nadu, INDIA.
[5]Department of Physics, Nehru College of Engineering and Research Centre, Pampady, Thrissure, Kerala, INDIA

ABSTRACT

The ZnO-TiO_2 nanocomposites were prepared by means of sol-gel method XRD patterns reveal the formation of well-crystalline single phase materials. It is found that the crystallite size has been reduced due to addition of TiO_2 in ZnO matrix as compared with ZnO nanoparticles. The synthesized ZnO-TiO_2 nanoparticles have been characterized by using X-ray diffraction (XRD), UV-Visible spectroscopy, Photoluminescence, Vibrating sample magnetometer instruments and the morphologies were observed with FESEM and TEM.

Keywords: ZnO-TiO_2, XRD, UV-Visible spectroscopy, FESEM and TEM

INTRODUCTION

Metal oxide nanoparticles attract great attention in recent years on account of their special electronic and chemical properties. Among the metal oxide semiconductors, ZnO and TiO_2 have been investigated extensively due to their chemical stability and efficient photocatalytic properties. Zinc oxide has achieved applications in various areas such as optical, piezoelectric, magnetic, and gas sensing properties, and apart from this, zinc compounds have been generally regarded as safe [1]. Titanium oxide (TiO_2) is the most widely used metal oxide for environmental applications, paints, electronic devices [2], gas sensors [3] and solar cells [4, 5]. It is well known semiconductor with excellent photocatalytic property that has been widely used in environmental pollutant elimination [6, 7], antibacterial dopes, self-clean buildings, etc. [8]. Its unique antibacterial properties make the material a candidate for applications in medical devices and sanitary ware surfaces. However, there are still problems needed to be dissolved concerning its application in photocatalysis. For most of the photocatalytic decomposition processes, photonic efficiency is relatively low, and furthermore, photocatalytic reactions on TiO_2 nanoparticles can usually be induced only by ultraviolet light, which limits the application of TiO_2 as a photocatalyst with visible light [9]. It is expected that the composites of ZnO and TiO_2 would exhibit useful applications in photocatalysis. As to this, recently, several papers concerning the enhancing of TiO_2 photocatalytic activity have been reported. Most of them concern modifying the photocatalysts by doping with ions [10, 11], or coupling TiO_2 to other oxides [12] for instance to ZnO [13]. Coupled semiconductor photocatalyst of TiO_2/ZnO has been investigated to enhance the photodegradation efficiency of TiO_2 catalyst by a number of researchers and its effect for improving photocatalytic efficiency was reported [9, 13-15]. On the

contrary, some studies found that coupling of ZnO and TiO_2 semiconducting powders was not so beneficial to enhance the photoreactivity for the studied reaction [16]. Research in this area is of both scientific and applied significance.

In this research work, ZnO-TiO_2 nanocomposites were synthesized by sol-gel method. The synthesized ZnO nanoparticles have been characterized by using X-ray diffraction (XRD), UV-Visible spectroscopy, Photoluminescence, Vibrating sample magnetometer instruments and the morphologies were observed with FESEM and TEM.

Experimental Details

Materials and Methods

The chemicals such as zinc chloride, titanium tetrachloride, ethanol and benzyl alcohol were purchased in analytical grade and all the chemicals were used as such without any further purification.

The ZnO-TiO_2 nanocomposites were prepared by means of sol-gel method. For the preparation of, 1M zinc chloride was dissolved in 10 ml ethanol and the obtained solution was added to 50 ml benzyl alcohol under continuous stirring at room temperature. Since, benzyl alcohol serves as both the solvent and the reagent to interact with various metal chlorides for the synthesis of a series of metal oxides and compound oxides. To this mixture, 1M $TiCl_4$ was slowly added. The obtained orange liquid was stirred continuously at 60°C for 8 hours. Thus obtained materials were left for aging at room temperature. The resulting white thick suspensions were centrifuged at 4500 rpm for 15 min and the supernatant was discarded by decantation. The white precipitates were then washed two times with absolute ethanol and three times with diethyl ether. After every washing step, the solvent was separated by centrifugation. The collected material was dried in air overnight and then ground into a fine powder. The obtained powders were calcinated at 200°C which yields to ZnO-TiO_2 nanocomposites. Figure 1 summarizes the steps involved in the synthesis of ZnO-TiO_2 nanocomposites.

CHARACTERIZATION METHOD

The structure of the prepared ZnO-TiO_2 nanocomposites was investigated from the X-ray diffraction patterns obtained using a Riagu Mini Flexell Desktop Diffractometer (using CuKα radiation at a wavelength of 1.5406 Å). Optical properties were studied using UV-VIS spectrophotometer (JASCO -V-670) in the wavelength range of 300 - 1000 nm. Photoluminescence measurements were taken using Photoluminescence spectrometer (HORIBA Jobin Yvon) with 325 nm He-Cd laser. The magnetic properties of the doped thin films were studied using Lake Shore 7404 vibrating sample magnetometer instrument. The morphologies were observed by JEOL 7001F Field emission scanning electron microscope (FESEM) equipped with EDS to find the elemental composition. TEM images with SAED patterns were observed using JEOL JEM 2100 Transmission electron microscope.

Structural analysis

The XRD patterns of the ZnO-TiO_2 nanocomposites are shown in Figure 2. The XRD patterns reveal the formation of well-crystalline materials. The obtained XRD patterns of the ZnO-TiO_2 nanocomposites were compared with the standard data for ZnO (JCPDS card No. 80-0075) and TiO_2 (JCPDS card No. 89-4921).

The diffraction peaks shown at planes 100, 002, 101, 102, 110, 103, 200, 112, 201 and 202 corresponds to ZnO hexagonal wurtzite phase. In addition, peaks at 101, 004, 200, 105 and 211 planes are in correspondence with TiO_2 anatase phase diffraction peaks. Since there was complete incorporation of Ti into the ZnO structure [17]. From the observed peaks the corresponding planes were indexed in Figure 2. Furthermore, the intensity of the ZnO peaks decreased due to TiO_2 fused to the ZnO matrix.

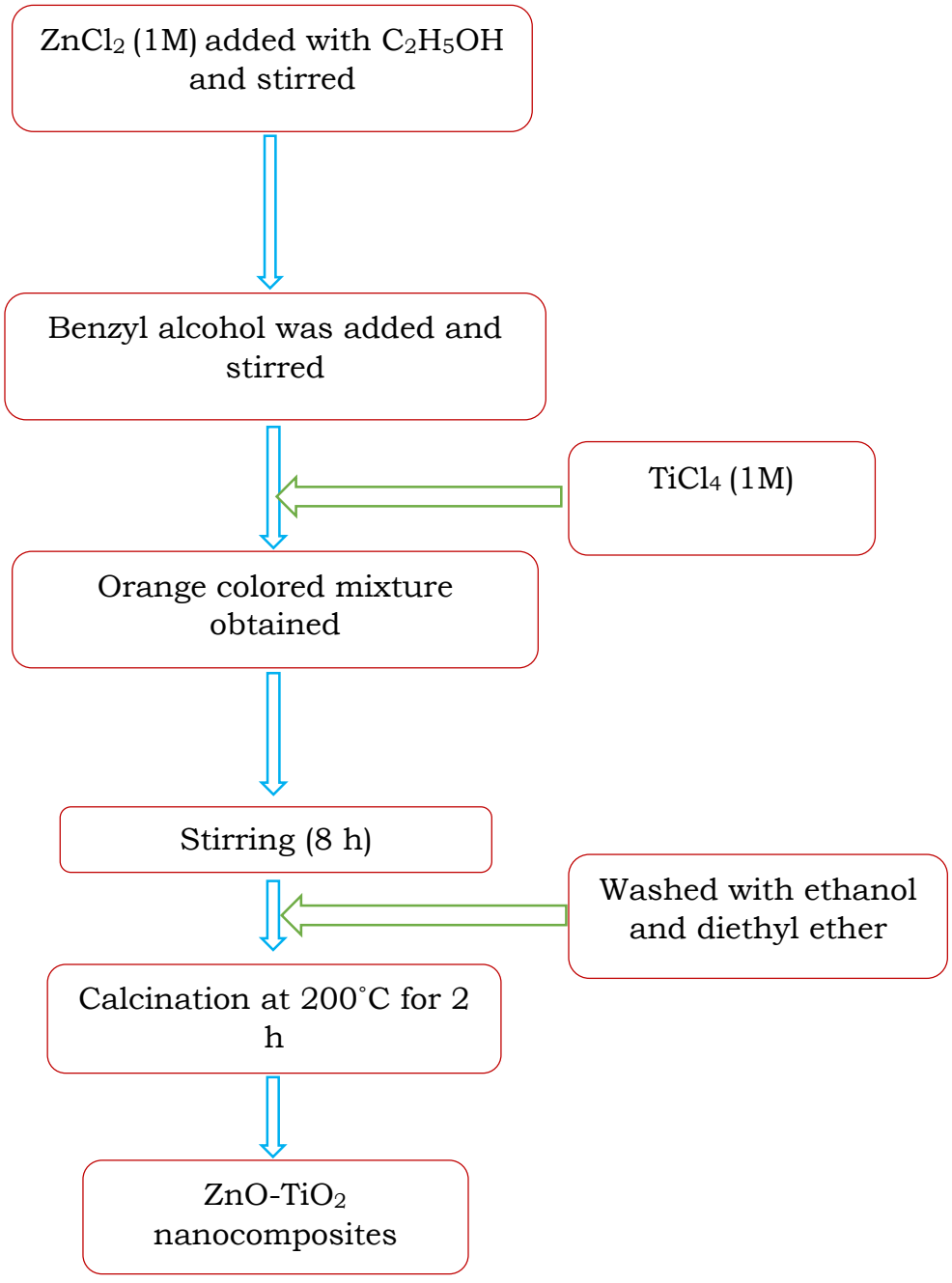

Figure 1 Steps involved in the synthesis of ZnO-TiO_2 nanocomposites

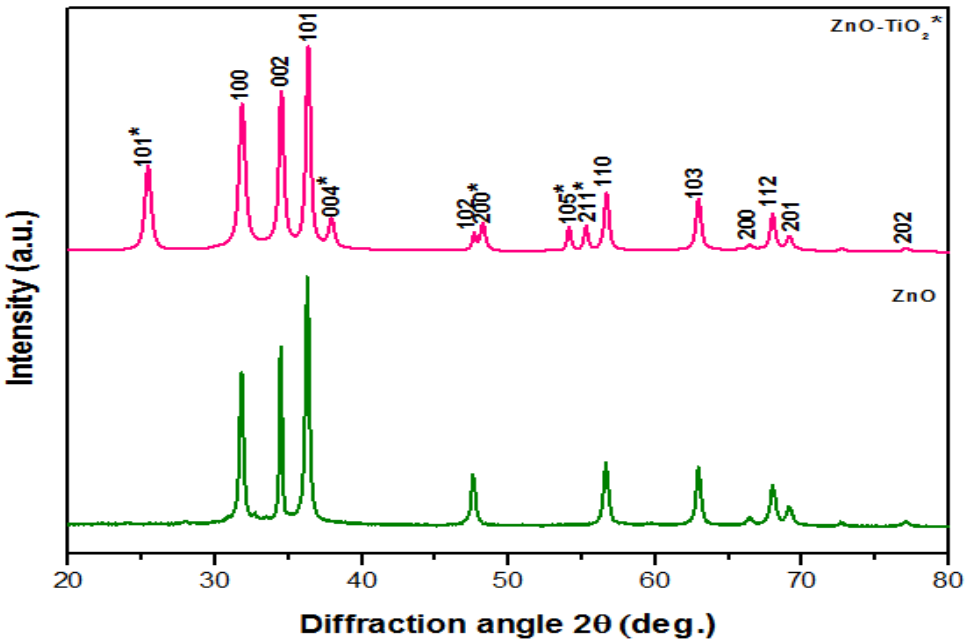

Figure 2 The XRD patterns of ZnO-TiO_2 nanocomposites

The crystallite size has been calculated using Scherer's formula from the XRD data and presented in Table 4.1.

$$D = \frac{K\lambda}{\beta \, Cos \, \theta} \, (nm)$$

The dislocation density (δ) is estimated using the equations,

$$\delta = \frac{15 \, \beta \, cos\theta}{4\alpha D} \quad lines \, / \, m^2$$

Micro strain (ε) were calculated using,

$$\varepsilon = \frac{\beta}{4 \tan \theta}$$

The existence of stacking faults gives rise to a shift in a peak position of different reflection planes with respect to an ideal position of fault free sample. The relation between stacking faults probability *(α)* with peak shift in terms of (*β)* is given by

$$\alpha = \left[\frac{2\pi^2}{45(3 \tan \theta)^{\frac{1}{2}}}\right] \beta \, (\text{Å})$$

where,*α* - is the stacking fault

β - is the full width at half maximum

From Table 1, it is found that the crystallite size has been reduced due to addition of TiO_2 in ZnO matrix as compared with pure ZnO nanoparticles. The dislocation density are found to be decreased with increase in crystallite size. Furthermore from the calculations, the stacking fault and elastic strains are found to be decreased with increase in crystallite size. XRD studies showed that, ZnO-TiO_2 nanocomposites has good crystalline nature, less dislocation, stacking fault and elastic strains. The small value of dislocation density confirms that the sol-gel method is an effective technique for good quality poly crystalline ZnO-TiO_2 nanocomposites.

Table 1 Structural parameters of ZnO-TiO_2 nanocomposites

Planes	Crystallite Size D (nm)	Dislocation Density (δ) (10^{15} lines / m^2)	Stacking faults probability (Å)	Elastic strains Ɛ
100	18.24	5.0254	0.0039	0.0072
002	22.51	3.2985	0.0031	0.0054
101	24.22	2.8512	0.0028	0.0048
101*	17.06	5.7419	0.0046	0.0097
004*	21.32	3.6777	0.0031	0.0052
200*	23.58	3.0080	0.0025	0.0038

Optical properties

The optical absorption spectra of ZnO-TiO_2 nanocomposites demonstrate a displacement of the absorption band edge into the visible region was shown in Figure 3. The variations in absorbance can be explained taking into account the formation of agglomerates in the suspension that, when sediment cause a decrease in absorbance, a behavior more evident in the titanium-doped ZnO samples. The maximum absorption of wavelength near 380 nm was found and attributed to electronic transitions involve states located in the energy gap, generated by the defects present in the structure of the synthesized sample,, which is related to the bandgap of ZnO-TiO_2 nanocomposite powder. Red shift is observed in the absorption edge with increasing the volume ratio of TiO_2 into the ZnO. This may be related to particle size, surface morphology and variation with increasing the volume ratio of TiO_2. This red shift causes variation in the Fermi level of ZnO:TiO_2 nanocomposites lead to energy bandgap decreased. The band located at ∼270 nm ware observed in the spectra. These might correspond to electronic transitions from the deep levels of the valence band or indicate effects of quantum confinement due to the nanometer size of the particles [18].

The band gap values of the sample are determined using the Tauc plot analysis. The optical band gap values have been calculated using the fundamental absorption, which corresponds to electron

excitation from the valence band to the conduction band. The relation between absorption coefficient α and incident photon energy (hv) are given by the equation

$$(\alpha h\nu) = A(h\nu - E_g)^n$$

where, A is a constant, E_g is the bandgap of the material and the exponent n depends on the type of transition.

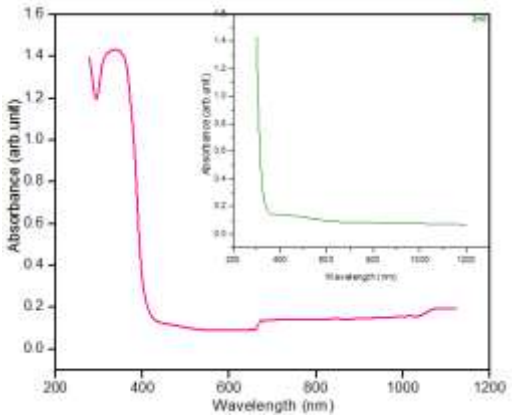

Figure 3 Optical absorbance spectra of ZnO-TiO_2 nanocomposites

Tauc plots between $(\alpha h\nu)^2$ and energy have been plotted and the linear portions of the graphs were extrapolated to meet the energy axis as shown from Figure 4 from which the energy band gap have been determined as 3.05 eV. The inset picture show the energy bandgap of pure ZnO. Bandgap was decreased in ZnO-TiO_2 due to expansion of the conduction and valance bands of ZnO and it is attributed to the variation of TiO_2 volume ratio in ZnO, which leads to modification in band gap 3.48 eV (pure ZnO) to 3.05 eV and was analogous to the interaction between ZnO and TiO_2. This shift shows the electronic structure (band-band transitions or HOMO-LUMO transitions) have been modified by doping material [19-20].

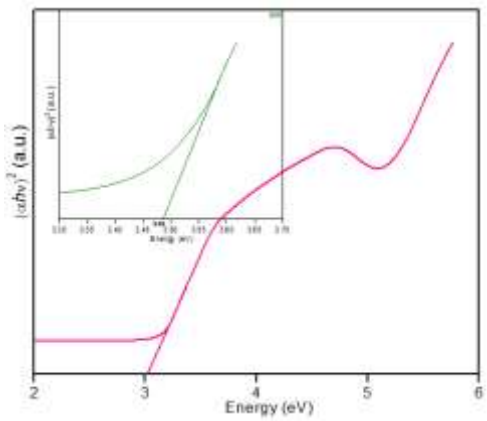

Figure 4 Optical bandgap of ZnO-TiO_2 nanocomposites

Photoluminescence spectroscopy

ZnO-TiO_2 nanocomposites superposition of the photoluminescence (PL) spectra was shown in Figure 5. Observing the PL spectra, there are two well defined regions, one peak in UV region 430 nm of high intensity and another in visible region 615 nm of the spectrum with low intensity. The UV region peak at 430 nm corresponds to near band edge emission (NBE) which is due to exciton-related transitions and visible region peak 615 nm appears because of crystal defects like Zn interstitials and oxygen vacancies. However, when TiO_2 was incorporated to the structure, the UV peak was observed to be shifted towards comparatively larger wavelength (red shift) because of the change in electronic structure and that in the band gap of the doped structures. Upon doping, impurity states are created below the conduction band due to which red shift appears. This is because of the change of size of dopant and the host material which produced defects due to which visible luminescence become improved. The oxygen vacancies and intrinsic defects may be considered responsible for the origin of orange band near 615 nm. The observed orange emission is also due to the impurity levels correspond to the singly ionized oxygen vacancy in ZnO. The peaks giving emissions at 430 nm is due to deexcitation from lower vibronic levels in Ti^{3+} 3d states of ZnO-TiO_2 lattice to the deep trap levels (acceptor). The emission wavelengths at 615nm are due to deexcitation from lower vibronic levels in deexcitation from lower vibronic levels in the oxygen vacancies of TiO_2 lattice to the ground state. It can be concluded that the defects in the samples of ZnO-TiO_2 nanocomposites were: O_i, Zn_i, V_O and V_{Zn} [21-22].

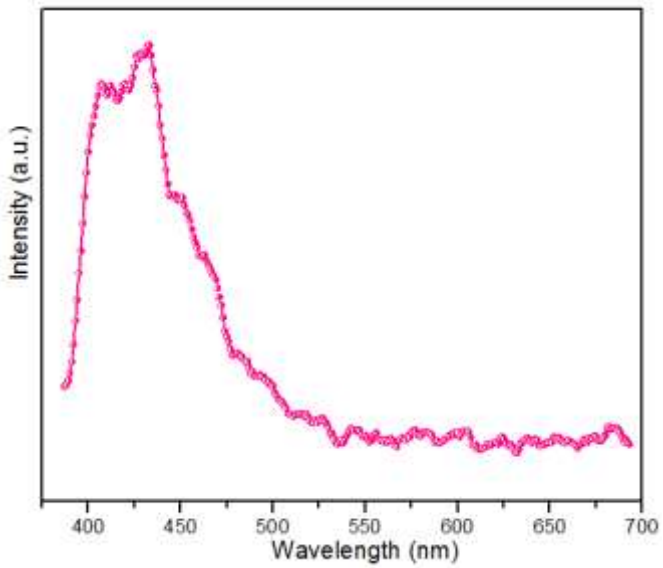

Figure 5 Photoluminescence (PL) spectra of ZnO-TiO_2 nanocomposites

Vibrating Sample Magnetometry (VSM) measurements

The magnetic behavior of the ZnO-TiO_2 nanocomposites was investigated by plotting the magnetic moment as a function of the applied magnetic field measured while the magnetic properties obtained

from the hysteresis loop are shown in Figure 6. The inset picture shows the diamagnetic behavior of ZnO. The observed curve shows a hysteresis, which indicates the existence of ferromagnetic ordering in the sample. The particle size of 21 nm obtained was less than the critical nanoparticle size (100 nm); consequently the nanoparticles form single domains with all the spins aligned in the same direction and uniformly magnetized. Furthermore, because there are no domain walls to move, the magnetization will be reversed through spin rotation rather than through the motion of domain walls which results in large coercivity of the nanoparticles. However observed coercivity (magnetic field required to bring the magnetization back to zero) is relatively small suggesting that the nanoparticles are spherical. This observation is in conformity with the SEM results which suggested that the ZnO-TiO_2 nanocomposites were spherical. At such low coercivity, the ferromagnetic nanoparticles with possible coexistence of paramagnetism behave like paramagnetic atoms with giant spins, and as the coercivity turns to zero, the nanoparticles become super magnetic [23].

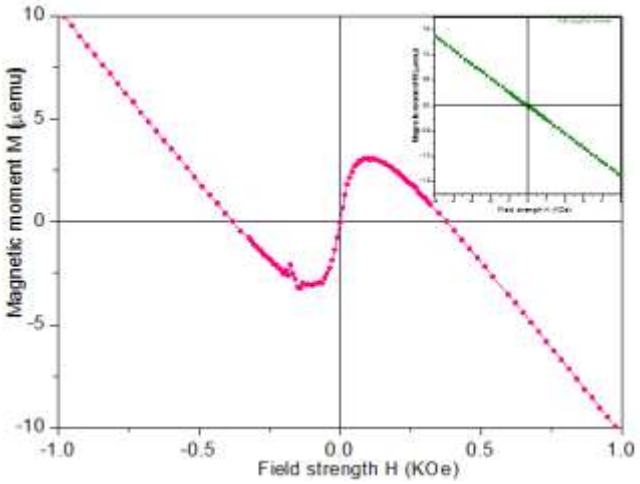

Figure 6 M–H curves of ZnO-TiO_2 nanocomposites

SEM and EDS Analysis

Scanning electron micrograph was shown in Figure 7a. The SEM images of the ZnO-TiO_2 nanocomposites have spherical in shape. This spherical in shape are due to the TiO_2 incorporated in ZnO matrix. From the SEM photographs, the sample have a uniform particle distribution. With the aid of Image processing tools the quantitative analysis of porosity and of pores dimension were processed. Fig. 7b is the intensity map of the image after multilevel thresholding with 6 level of quantization. In Fig. 7c the darkest portion of the image is selected and shown with white pixels in a solid black background. Fig. 7d shows the segmented porous space of ZnO samples labeled with different random colors. The pore size distributions are illustrated in 7e.

Fig. 7a and Fig. 7d shows the original and final processed images for ZnO-TiO_2 nanocomposites. ZnO-TiO_2 nanocomposites have a distribution with less frequency ratio which denotes the larger pore sizes as compared with ZnO prepared using precursors $ZnCl_2$. The porosity, average and standard deviation of the pore sizes are found to be 0.2664 %, 2.6626 nm and 1.7091 nm. As compared with ZnO (0.2754 %),

the porosity of nanocomposites (0.2664 %) is decreased due to addition of TiO_2 with in ZnO matrix. Porosity typically decreases as particle size increases. This is due to chemical aggregate formation in finer textured surface when subject to synthesis processes.The reduced porosity and the size of the pathways are more tightly packed the sediment to the lower permeability. The Average pore radius value of the synthesized composites were identified as mesoporous materials and used for solar cell applications.

Figure 8 shows the 3D surface roughness (grey scale (a) and color (b)) of the ZnO-TiO_2 nanocomposites which was revealed from SEM images using image processing tools. It is found that the surface roughness is decreased as compared with ZnO prepared with zinc chloride. This is due to porosity ratio is low for this nanocomposite compared ZnO prepared with zinc chloride. So it can be concluded that surface roughness is directly proportional to the porosity.

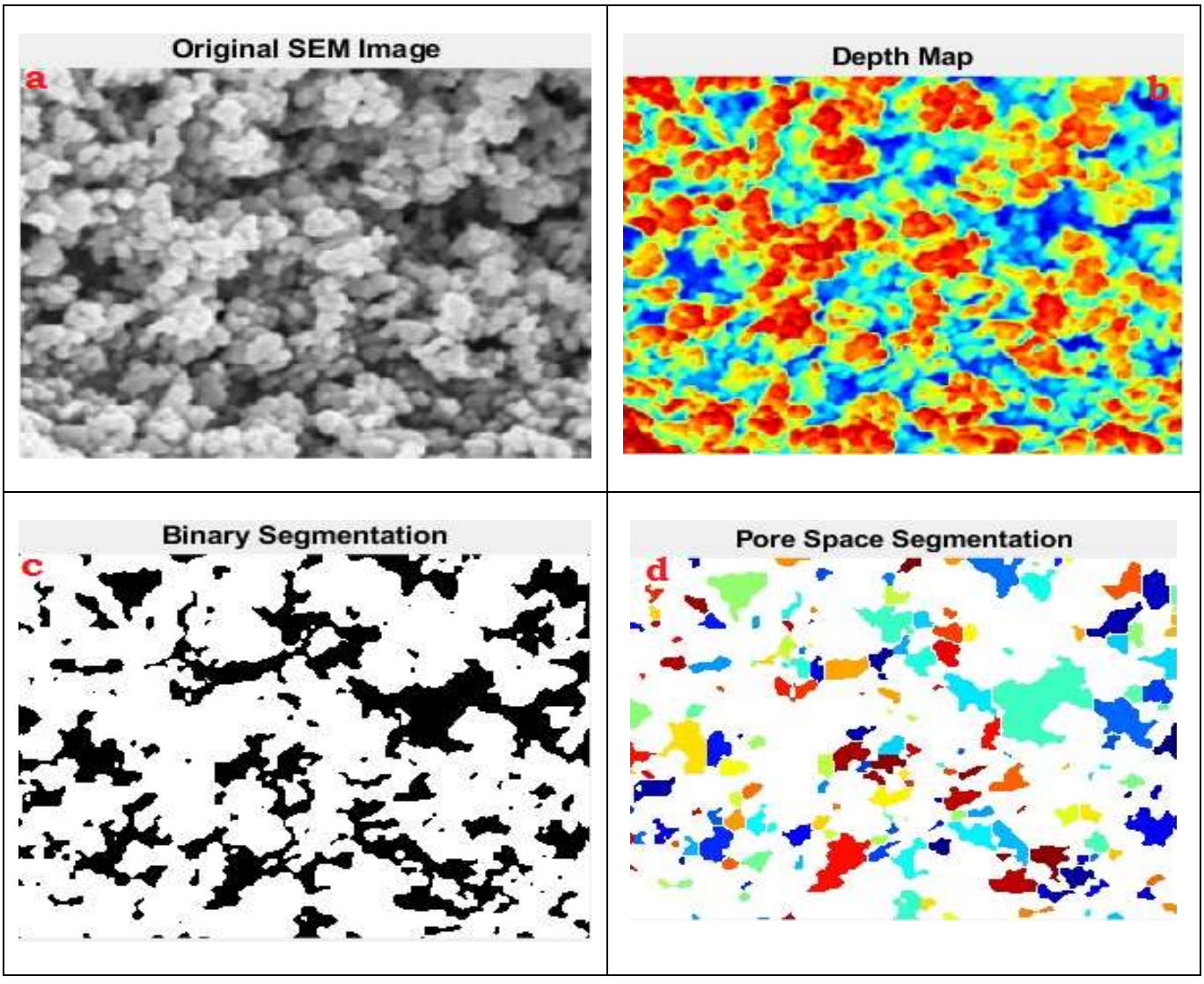

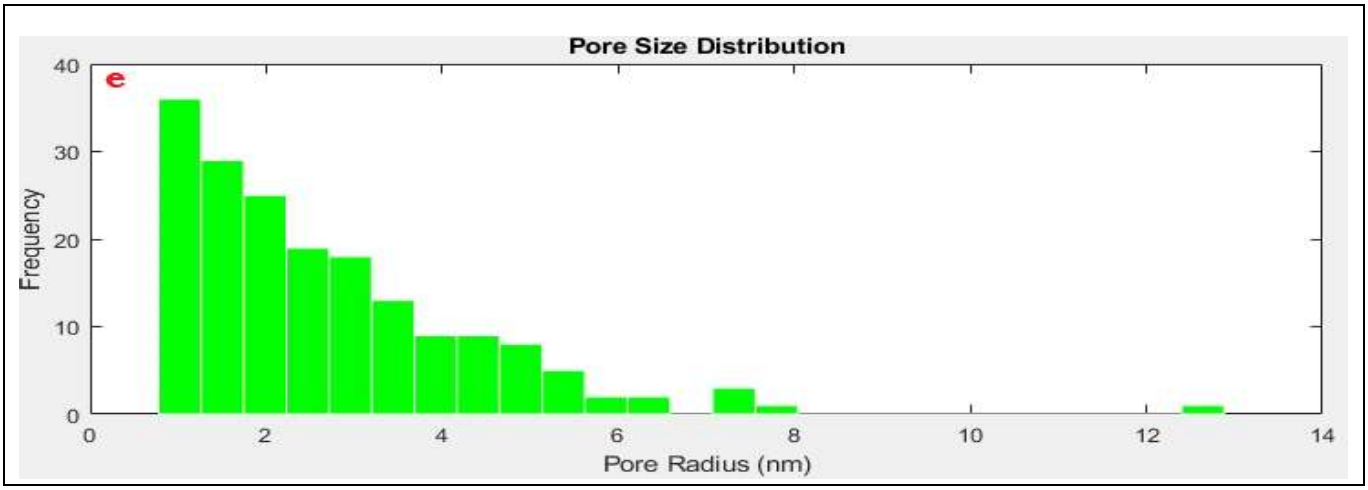

Figure 7 SEM micrographs of ZnO-TiO_2 nanocomposites

EDS spectra recorded during the SEM imaging technique and are shown in Figure 9. The peaks around 1.01 and 1.03keV are from the Zn La and Lb lines, and peaks observed with less counts are observed at 8.6 keV and 9.6 keV are due to Zn Ka and Zn Kb line. . The peaks around 0.5keV are from the O Ka lines. The peaks around 0.452 and 0.458 keV are from the Ti La and Lb lines, and peaks observed at 4.5 keV and 4.9 keV are due to Ti Ka and Ti Kb line. It is because the incident electron will remove a Ti K-shell electron, electrons fall back from L and M shells to give discreet X-ray quanta from L to K gives Ti Ka1 at 4.5 keV and from L to K gives Ka2 (this line is not resolvable in EDX), the transition from M to K gives a higher energy line Ti Kb at 4.9 keV. The inset picture shows the EDS of ZnO. The intensity of Zn decreased by increase intensity of Ti is due to dopant was dispersed uniformly in the ZnO matrix. It is observed that the nanoparticles contain zinc, titanium and oxygen elements predominantly.

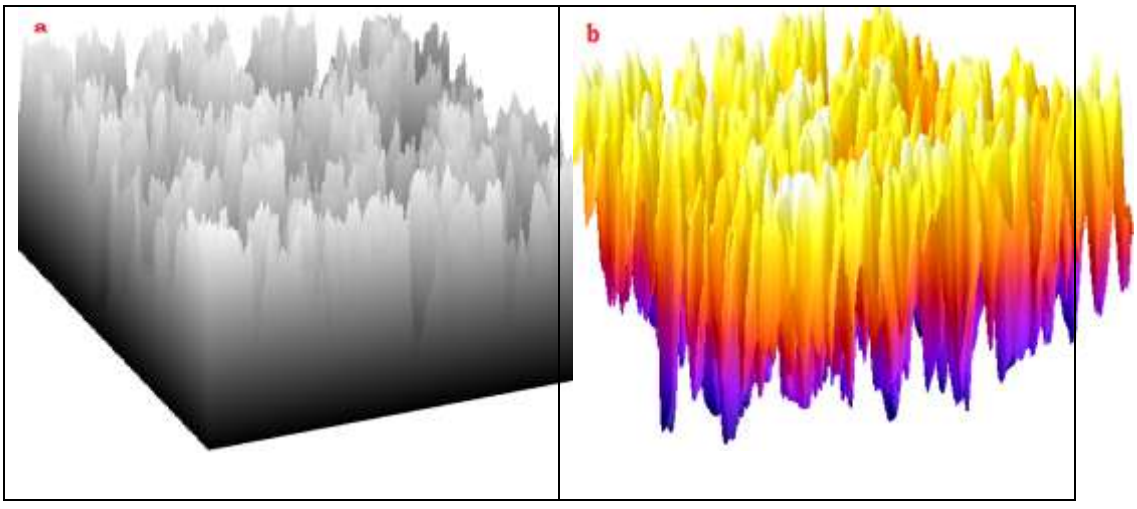

Figure 8 Surface roughness of ZnO-TiO_2 nanocomposites

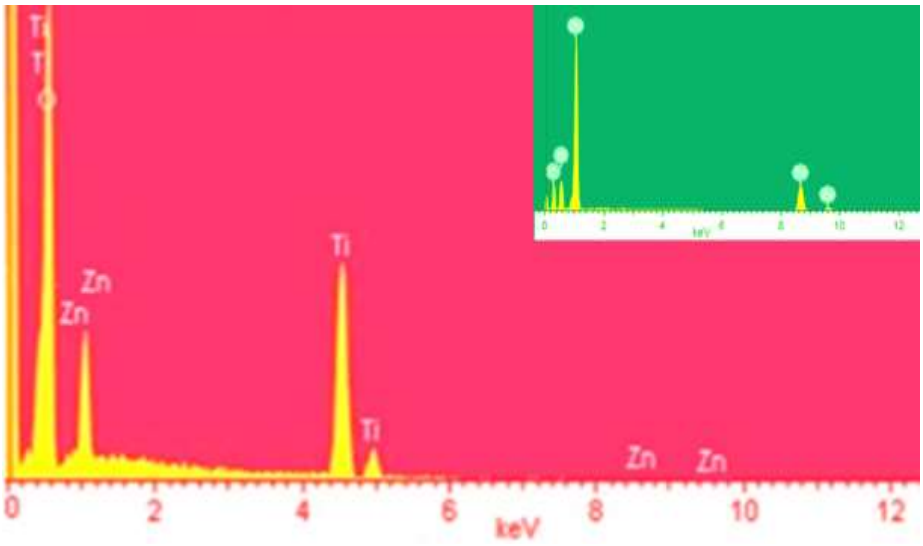

Figure 9 EDS of ZnO-TiO_2 nanocomposites

HRTEM analysis

HRTEM of the ZnO-TiO_2 nanocomposites is shown in Figure 10a. The nanocomposites exhibit in hexagonal facet and spherical like morphology with size of ~17-24 nm which confirms hexagonal wurtzite structure and small particles were decorated over the hexagonal facet and spherical structure. Image processing software tools were used to find the d spacing (Figure 10b) by employing Fast Fourier Transform (FFT) and Inverse Fast Fourier transform (IFFT) technique and confirms the d space value at plane 100 reveals 0.2810 nm which was in close match with the corresponding standard values, respectively. The results achieved from FFT technique were further filtered by applying Sobel filter tools to detect the defects (stacking fault and dislocation) and plotted in Figure 10c. The resultant micrograph were additionally processed to detect the defects in color image (Figure 10d). The clusters of bluish green lines represent the defects (stacking fault and dislocation).

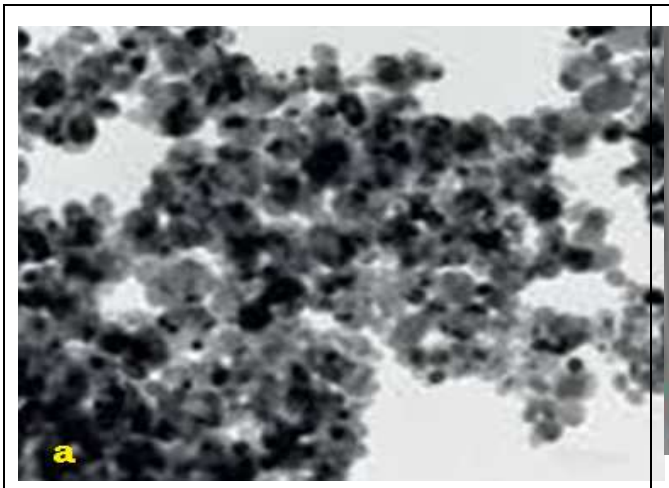

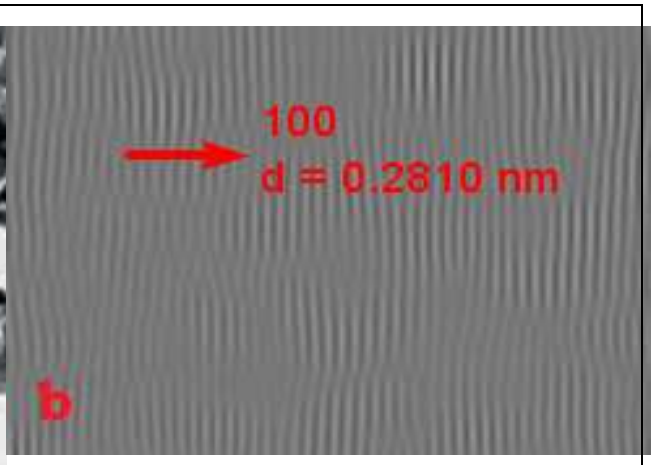

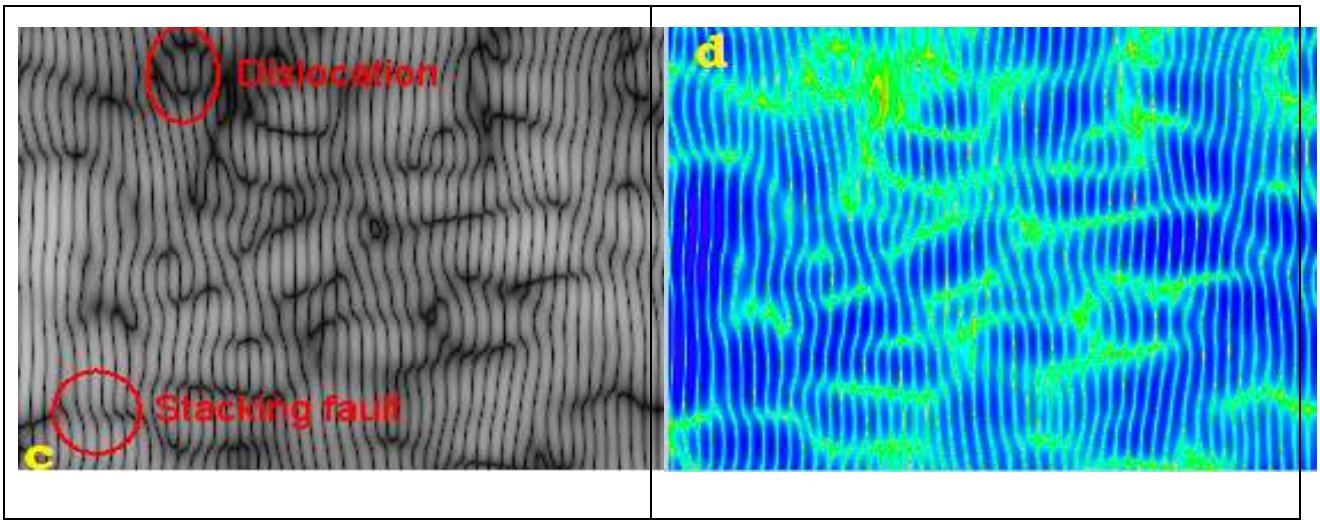

Figure 10 HRTEM micrographs of ZnO-TiO_2 nanocomposites

CONCLUSION

The ZnO-TiO_2 nanocomposites were prepared by means of sol-gel method by using zinc chloride, titanium tetrachloride, ethanol and benzyl alcohol. The XRD patterns reveal the formation of well-crystalline single phase materials. The diffraction peaks shown at planes 100, 002, 101, 102, 110, 103, 200, 112, 201 and 202 corresponds to ZnO hexagonal wurtzite phase. In addition, peaks at 101, 004, 200, 105 and 211 planes are in correspondence with TiO_2 anatase phase diffraction peaks. Since there was complete incorporation of Ti into the ZnO structure. it is found that the crystallite size has been reduced due to addition of TiO_2 in ZnO matrix as compared with ZnO nanoparticles. From the investigations of UV-Vis spectra, the excitonic absorption peak at 380 nm were observed and have sharp absorption edge which implies the lower particle size of ZnO. bandgap was decreased in ZnO-TiO_2 due to expansion of the conduction and valance bands of ZnO and it is attributed to the variation of TiO_2 volume ratio in ZnO, which leads to modification in band gap 3.48 eV (pure ZnO) to 3.05 eV and was analogous to the interaction between ZnO and TiO_2. In PL spectra, the peaks giving emissions at 430 nm is due to deexcitation from lower vibronic levels in Ti^{3+} 3d states of ZnO-TiO_2 lattice to the deep trap levels (acceptor). The emission wavelengths at 615nm are due to deexcitation from lower vibronic levels in deexcitation from lower vibronic levels in the oxygen vacancies of TiO_2 lattice to the ground state. VSM study shows, the observed curve shows a hysteresis, which indicates the existence of ferromagnetic ordering in the sample. From the SEM photographs, samples have a uniform particle shape and size. EDS result revealed that the synthesized nanocomposite contain zinc, titanium and oxygen elements predominantly. The nanocomposites exhibit in hexagonal facet and spherical like morphology with size of ~17-24 nm which confirms hexagonal wurtzite structure. The Average pore radius value of the synthesized composites were identified as mesoporous materials and used for solar cell applications.

REFERENCES

[1] Wahab, R., Mishra, A., Yun, S.I., Kim, Y.S. and Shin, H.S., "Antibacterial activity of ZnO nanoparticles prepared via non-hydrolytic solution route", Applied microbiology and biotechnology, 87(5), 2010, 1917-1925.

[2] Zhang, C., Yu, P.L., Li, Y. and Li, J.C., "Polymer/TiO_2 Nanoparticles interfacial effects on resistive switching under mechanical strain", Organic Electronics, 77, 2020, 105528.

[3] Rzaij, J.M. and Abass, A.M., "Review on: TiO_2 Thin Film as a Metal Oxide Gas Sensor", Journal of Chemical Reviews, 2(2), 2020, 114-121.

[4] Maurya, I.C., Singh, S., Senapati, S., Srivastava, P. and Bahadur, L., "Green synthesis of TiO_2 nanoparticles using Bixa orellana seed extract and its application for solar cells", Solar Energy, 194, 2019, 952-958.

[5] Aboulouard, A., Gultekin, B., Can, M., Erol, M., Jouaiti, A., Elhadadi, B., Zafer, C. and Demic, S., "Dye sensitized solar cells based on titanium dioxide nanoparticles synthesized by flame spray pyrolysis and hydrothermal sol-gel methods: a comparative study on photovoltaic performances", Journal of Materials Research and Technology, 9(2), 2020, 1569-1577.

[6] Sun, C., Wang, S., Ji, G., Wu, H., Huang, F. and Lv, J., "Characterizations and enhanced photocatalytic property of disorder-engineered TiO_2 nanomaterials", Ferroelectrics, 529(1), 2018, 149-158.

[7] Qin, R., Meng, F., Khan, M.W., Yu, B., Li, H., Fan, Z. and Gong, J., "Fabrication and enhanced photocatalytic property of TiO_2-ZnO composite photocatalysts", Materials Letters, 240, 2019, 84-87.

[8] Moradi, S., Aberoomand-Azar, P., Raeis-Farshid, S., Abedini-Khorrami, S. and Givianrad, M.H., "The effect of different molar ratios of ZnO on characterization and photocatalytic activity of TiO2/ZnO nanocomposite", Journal of Saudi Chemical Society, 20(4), 2016, 373-378.

[9] Hakki, H.K., Allahyari, S., Rahemi, N. and Tasbihi, M., "Surface properties, adherence, and photocatalytic activity of sol–gel dip-coated TiO_2–ZnO films on glass plates", Comptes Rendus Chimie, 22(5), 2019, 393-405.

[10] Diamandescu, L., Vasiliu, F., Tarabasanu-Mihaila, D., Feder, M., Vlaicu, A.M., Teodorescu, C.M., Macovei, D., Enculescu, I., Parvulescu, V. and Vasile, E., "Structural and photocatalytic properties of iron-and europium-doped TiO_2 nanoparticles obtained under hydrothermal conditions", Materials Chemistry and Physics, 112(1), 2008, 146-153.

[11] Tong, T., Zhang, J., Tian, B., Chen, F. and He, D., "Preparation of Fe3+-doped TiO_2 catalysts by controlled hydrolysis of titanium alkoxide and study on their photocatalytic activity for methyl orange degradation",Journal of Hazardous Materials, 155(3), 2008, 572-579.

[12] Sabzehei, K., Hadavi, S.H., Bajestani, M.G. and Sheibani, S., "Comparative evaluation of copper oxide nano-photocatalyst characteristics by formation of composite with TiO_2 and ZnO", Solid State Sciences, 107, 2020,106362.

[13] Çırak, B.B., Caglar, B., Kılınç, T., Karadeniz, S.M., Erdoğan, Y., Kılıç, S., Kahveci, E., Ekinci, A.E. and Çırak, Ç., "Synthesis and characterization of ZnO nanorice decorated TiO_2 nanotubes for enhanced photocatalytic activity",Materials Research Bulletin, 109, 2019, 160-167.

[14] Xu, X., Wang, J., Tian, J., Wang, X., Dai, J. and Liu, X., "Hydrothermal and post-heat treatments of TiO_2/ZnO composite powder and its photodegradation behavior on methyl orange", Ceramics International, 37(7), 2011, 2201-2206.

[15] Haffad, S. and Kiprono, K.K., "Interfacial structure and electronic properties of TiO_2/ZnO/TiO_2 for photocatalytic and photovoltaic applications: A theoretical study", Surface Science, 686, 2019, 10-16.

[16] Marci, G., Augugliaro, V., López-Muñoz, M.J., Martín, C., Palmisano, L., Rives, V., Schiavello, M., Tilley, R.J. and Venezia, A.M., "Preparation characterization and photocatalytic activity of polycrystalline ZnO/TiO_2 systems. 1. Surface and bulk characterization", The Journal of Physical Chemistry B, 105(5), 2001, 1026-1032.

[17] Shalaby, A., Dimitriev, Y., Iordanova, R., Bachvarova-Nedelcheva, A. and Iliev, T., "Modified sol-gel synthesis of submicron powders in the system ZnO-TiO_2", Journal of the University of Chemical Technology and Metallurgy, 46(2), 2011, 137-142.

[18] Goh, E.G., Xu, X. and McCormick, P.G., "Effect of particle size on the UV absorbance of zinc oxide nanoparticles", Scripta Materialia, 78, 2014, 49-52.

[19] Mallika, A.N., Reddy, A.R. and Reddy, K.V., "Annealing effects on the structural and optical properties of ZnO nanoparticles with PVA and CA as chelating agents", Journal of Advanced ceramics, 4(2), 2015, 123-129.

[20] Tam, K.H., Cheung, C.K., Leung, Y.H., Djurišić, A.B., Ling, C.C., Beling, C.D., Fung, S., Kwok, W.M., Chan, W.K., Phillips, D.L. and Ding, L., "Defects in ZnO nanorods prepared by a hydrothermal method", The Journal of Physical Chemistry B, 110(42), 2006, 20865-20871.

[21] Wu, X.L., Siu, G.G., Fu, C.L. and Ong, H.C., "Photoluminescence and cathodoluminescence studies of stoichiometric and oxygen-deficient ZnO films", Applied Physics Letters, 78(16), 2001, 2285-2287.

[22] Djurišić, A.B. and Leung, Y.H., "Optical properties of ZnO nanostructures", small, 2(8-9), 2006,944-961.

[23] Etape, E.P., Foba-Tendo, J., Ngolui, L.J., Namondo, B.V., Yollande, F.C. and Nguimezong, M.B.N., "Structural Characterization and Magnetic Properties of Undoped and Ti-Doped ZnO Nanoparticles Prepared by Modified Oxalate Route", Journal of Nanomaterials, 2018, 9072325(9).